PROCEEDINGS OF SPIE

SPIEDigitalLibrary.org/conference-proceedings-of-spie

Properties of resonant photonic lattices: Bloch mode dynamics, band flips, and applications

Magnusson, Robert, Lee, Kyu J., Hemmati, Hafez, Bootpakdeetam, Pawarat, Vasilyev, Jonathan, et al.

Robert Magnusson, Kyu J. Lee, Hafez Hemmati, Pawarat Bootpakdeetam, Jonathan Vasilyev, Fairooz A. Simlan, Nasrin Razmjooei, Yeong Hwan Ko, Shanwen Zhang, Sun-Goo Lee, Halldor G. Svavarsson, "Properties of resonant photonic lattices: Bloch mode dynamics, band flips, and applications," Proc. SPIE 11290, High Contrast Metastructures IX, 1129006 (26 February 2020); doi: 10.1117/12.2547322



Event: SPIE OPTO, 2020, San Francisco, California, United States

Properties of resonant photonic lattices: Bloch mode dynamics, band flips, and applications

Robert Magnusson, Kyu J. Lee, Hafez Hemmati, Pawarat Bootpakdeetam, Jonathan Vasilyev, Fairooz A. Simlan, Nasrin Razmjooei, and Yeong Hwan Ko Department of Electrical Engineering, University of Texas at Arlington, Arlington, Texas 76019, USA

Shanwen Zhang

Changchun Institute of Optics and Fine Mechanics and Physics, Chinese Academy of Sciences, Changchun, Jilin, 130033, China

Sun-Goo Lee

Advanced Photonics Research Institute, GIST, Gwangju 61005, South Korea Halldor G. Svavarsson

Reykjavik University, School of Science and Engineering, IS-101 Reykjavik, Iceland

ABSTRACT

We review guided-mode resonant photonic lattices by addressing their functionalities and potential device applications. The 1D canonical model is rich in properties and conceptually transparent, with all the main conclusions being applicable to 2D metasurfaces and periodic photonic slabs. We explain the operative physical mechanisms grounded in lateral leaky Bloch modes. We summarize the band dynamics of the leaky stopband. With several examples, we demonstrate that Mie scattering is not causative in resonant reflection. Illustrated applications include a wideband reflector at infrared bands as well as resonant reflectors with triangular profiles. We quantify the improved efficiency of a silicon reflector operating in the visible region relative to loss reduction as realizable with sample hydrogenation. A resonant polarizer with record performance is presented.

Keywords: guided-mode resonance effect, leaky-mode resonance, resonant waveguide gratings, metamaterials, Bloch modes, wave propagation in periodic media, leaky stopband dynamics, metasurfaces

1. INTRODUCTION

Optical or photonic lattices comprise a periodic assembly of arbitrarily shaped particles. These particles can be made of metals, dielectrics, and semiconductors or their hybrid compositions. The lattice is, in general, three-dimensional (3D) with important variants in the form of 2D or 1D patterned films. Thus, on account of the wide variety of material compositions and lattice architectures, the design space is vast. The utility of optical lattices is grounded in their ability to operate effectively on incident light to control and manipulate all key properties of the electromagnetic waves in play. This includes amplitude, phase, spectral distribution, polarization state, and local mode structure for light in the various available spectral regions. Due to ease of fabrication and spectral characterization, 1D and 2D films are intensely studied; these spatially modulated films are often called photonic crystal slabs, metasurfaces, or metastructures. Such surfaces may support lateral modes and localized field signatures with propagative and evanescent diffraction channels influencing the spectral response. As do all dielectric structures with nonzero refractive-index contrast at boundaries, the building-block particles can exhibit local Fabry-Perot and Mie mode signatures; however, upon resonance, lateral leaky Bloch modes sustained on the periodic particle assembly generate the functional response. A subwavelength restriction on the periodicity is usually maintained for efficient devices; however, it is also possible to generate interesting spectral behavior when this is not satisfied. The dominant second (leaky) stopband exhibits many remarkable physical properties including band-edge transitions and bound states in the continuum. The Fourier harmonic content of the spatial modulation is key to understanding the band dynamics of these lattices. Multi-resonance effects are observed when Bloch eigenmodes are

*magnusson@uta.edu; phone 1 817 272-2672; fax 1 817 272-2253; www.leakymoderesonance.com

High Contrast Metastructures IX, edited by Connie J. Chang-Hasnain, Andrei Faraon, Weimin Zhou, Proc. of SPIE Vol. 11290, 1129006 ⋅ © 2020 SPIE ⋅ CCC code: 0277-786X/20/\$21 ⋅ doi: 10.1117/12.2547322

excited with more than one evanescent diffraction channel. In this paper, we address the physical basis behind the fundamental resonance effects inherent in the lattice, discuss the observed behavior in connection with the lattice band structure, and show some example applications.

2. RESONANCE PHYSICS OF THE LEAKY-MODE LATTICE

Spatially patterned surfaces and films with subwavelength periodicity sustain dramatic resonance effects as input light couples to leaky Bloch-type waveguide modes [1-30]. Some 30 years ago, we coined the term "guided-mode resonance (GMR)" in an attempt to clearly communicate the fundamental physics governing these phenomena [30]. In earlier literature on the subject, authors often referred to these effects as being "anomalous," thereby implying that the phenomena were not well understood. In more recent literature, traditional periodic structures including GMR resonance devices in film format are frequently called photonic crystals, metasurfaces, or metamaterials [31-33]. It is very clear that GMR devices can have 1D or 2D lateral spatial modulation, or periodicity, as the resonance physics is not dependent on the type of periodicity in any fundamental way. The resonance effects of main interest here are observed in a slab, or film, geometry as the structure must be capable of supporting quasi-guided modes propagating laterally in the periodic lattice and hence being Bloch modes in common terminology. In the past, in the community of diffractive optics that preceded the metamaterials generation, such elements were sometimes called "waveguide gratings," a clear and physically-expressive descriptor. It has been well-known for a long time, on account of inherent design flexibility, that a plethora of differing spectral expressions is available with this device class, thus providing a facile applications platform. Indeed, wide parametric design spaces allow control of light amplitude, phase, polarization, near-field intensity, light distribution, etc., on surfaces and within device volumes. 3D variants of this device class are possible in which waveguide gratings are interspersed with homogeneous films forming an operational stack. There is presently much interest in subwavelength lattices and their applications [34-38].

2.1 Resonant spectral expressions: Mie scattering is not contributory

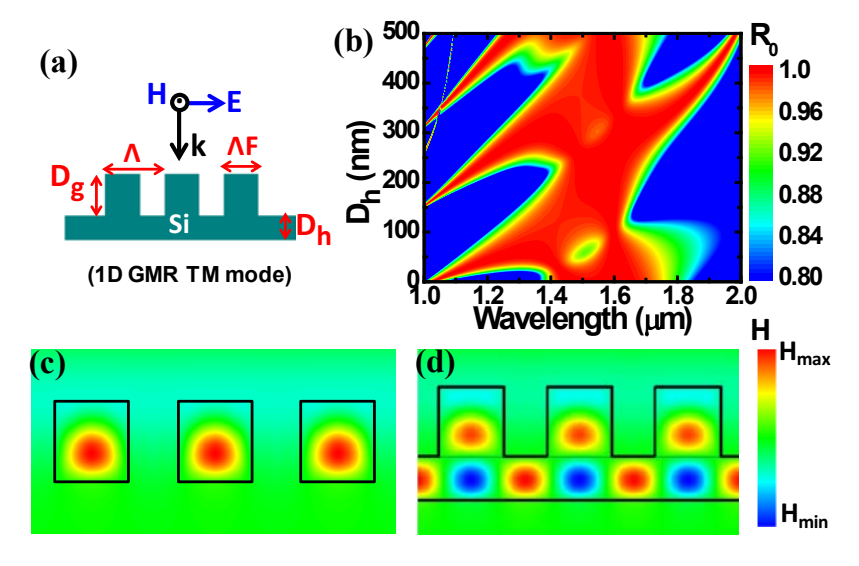


Figure 1. TM-polarized resonant reflector based on a 1D Si grating. The grating excites resonant leaky modes providing wide reflection bands. (a) The reflector designed with traditional grating parameters. (b) Calculated zero-order reflectance R_0 map as a function of the sublayer thickness. Cross-sectional views of the magnetic-field amplitude distribution appear in (c) for the grating with discrete ridges (D_h =0 nm) at λ = 1.62 μ m and in (d) for the grating imbued with a sublayer D_h =267 nm at λ = 1.55 μ m. After ref. 29.

Figure 1(a) depicts a silicon-based reflector under normal incidence in TM polarization with parameters defined as noted. The reflector works under guided-mode resonance (GMR), which arises when the incident wave couples to a leaky Bloch waveguide mode by phase matching with the second-order grating [6,7,10,11]. The 1D grating structure is identified by a parameter set { Λ =660 nm, F=0.6, D_g=430 nm, D_h} where the D_g and F are grating depth and fill factor. In the range 250 nm< D_h<350 nm, as shown in Fig. 1(b), the high reflection band is much wider than the band for the reflector consisting

of discrete parallel ridges (D_h =0 nm). The local field derives from interference between counterpropagating leaky modes, resulting in a standing-wave configuration. In Fig. 1(c), the field is localized in the isolated rods, whereas in Fig. 1(d), the guided lateral Bloch modes locate largely in the sublayer (D_h =267 nm). Fabry-Perot resonance and Mie scattering require discrete boundaries to support reflections and local field interactions. Discrete particle boundaries exist only at D_h = 0.

As an additional example, we provide Fig. 2 showing quantitatively that there is no fundamental difference between the resonance properties of 1D and 2D optical lattices. It illustrates a representative 2D GMR structure fashioned with high index (n_H) cylindrical grating film on a substrate (n_S) in a cover medium (n_C) where grating parameters include periods (Λ_x, Λ_y) , fill factors (F_x, F_y) , grating depth (d_g) , and homogeneous layer thickness (d_h) . Here, the d_h is critical to engineer the spectral response because it strongly affects guided modes in the sublayer coupled via diffraction. Figure 2(b) clearly shows that the reflectance properties depend on d_h as in Fig. 1 for the analogous 1D device. With optimal d_h , a wide bandwidth is achievable for high reflection. For $d_h = 0$ nm in Fig. 2(c), a wide flat-top band still appears since the grating layer supports leaky waveguide Bloch modes by itself. However, the optimal sublayer $(d_h = 68.3, \text{ or } 315 \text{ nm})$ achieves broader bandwidth while supporting lateral Bloch modes. In Fig. 2(d), the magnetic fields in the 2D grating with $d_h = 315$ nm illustrate local modes residing in the sublayer.

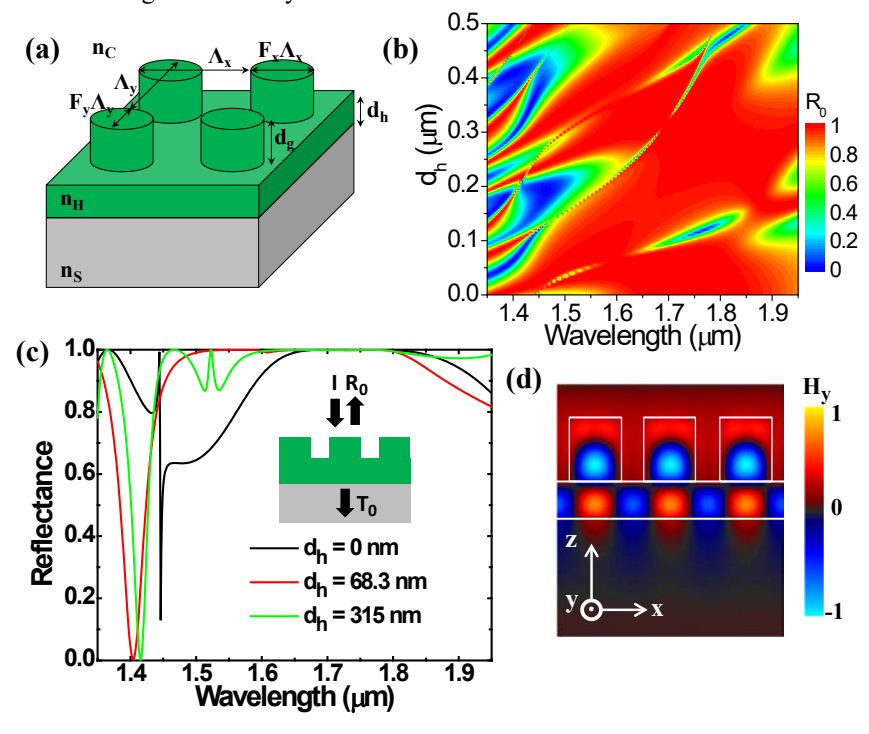


Figure 2. Unpolarized resonant reflector based on a 2D Si grating. (a) Model 2D GMR structure with grating parameters. (b) Color map of zero-order reflectance R_0 versus sublayer thickness (d_h0 . (c) Compared R_0 spectra for different d_h . (d) Magnetic field distribution of local modes in the 2D GMR device.

Fabry-Perot resonance and Mie scattering require discrete particle boundaries to support reflections and local field interactions. In the reflectors in Figs. 1 and 2, discrete boundaries are only in play when the homogeneous sublayer is zero. As the matched sublayer annihilates any localized resonances (Mie or Fabry-Perot) by destroying the resonance cavity, a Mie-resonance-based reflector should cease to function under this modification. From another point of view, connecting the individual particles with the sublayer should adversely alter the resonance dynamics. However, this is not the case, as evidenced by these results. In Fig. 1(b) for a 1D array of rectangular cylinders and in Fig. 2(b) for 2D pillars, there is a smooth change in the reflectance as the sublayer thickness rises, as evident in these figures. Indeed, these devices work very well under conditions where most of the resonant fields reside nearly entirely in the unmodulated sublayer. These conclusions are consistent with prior work showing that high-contrast interfaces and local Fabry-Perot resonances are not the root cause of wideband reflection observed in high-contrast gratings [20].

Media possessing high refractive indices may hold multiple leaky Bloch modes in a thin film that would be practical to deposit via sputtering for operation in the visible and near-IR regions. Silicon is a good example of such a medium as applied above. As the refractive index drops, attendant 1D or 2D grating contrast falls. GMR devices made with a low index typically exhibit narrow-band resonances. Figure 3(a) provides an example spectrum for a resonant membrane in air with a grating ridge refractive index of n_g =2. A resonance reflection results, with R_0 >0.99 at λ_{res} =1157 nm. The reflector has a parameter set { Λ =1000 nm, F=0.25, d_g =250 nm; TE polarization}; a Rayleigh anomaly appears at 1000 nm. Thus, an individual grating ridge is a rectangular rod with a cross section of 250 x 250 nm² and n_g =2. This combination will not support a Mie resonance at, or even near, the GMR wavelength. This conclusion is clear from the computed scattering cross section of an individual rod shown in Fig. 3(b). The Mie resonance is at ~700 nm or ~450 nm away from the GMR. This example is another demonstration of the noncausality of Mie scattering in resonance reflection.

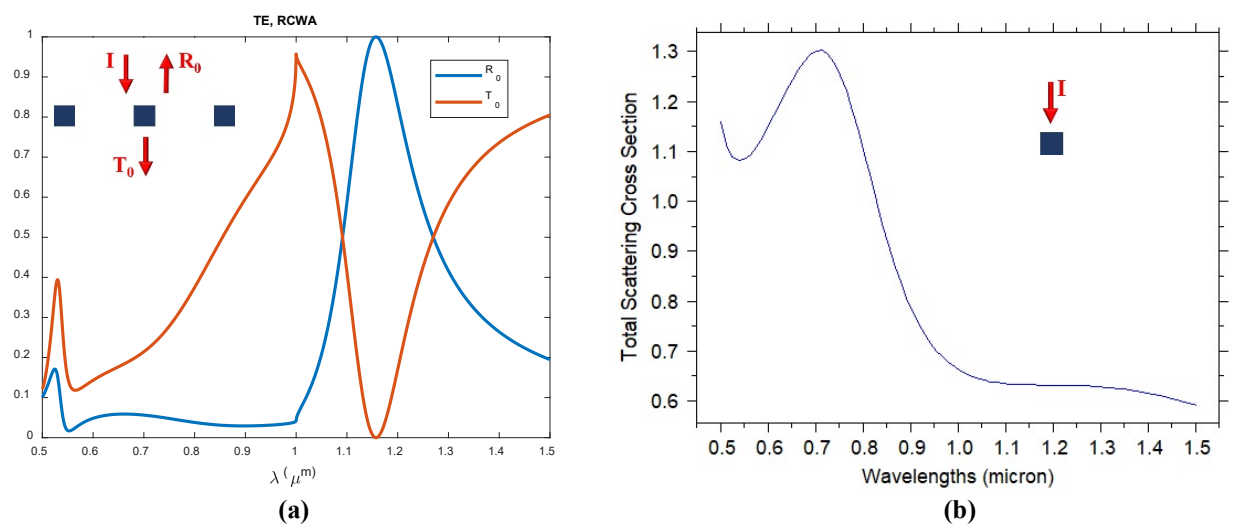


Figure 3. Demonstration of noncausality of Mie scattering in resonant reflection. (a) Reflection and transmission spectra for a low-index reflector membrane. (b) Scattering cross section for an elemental rod constituent of the reflector in (a).

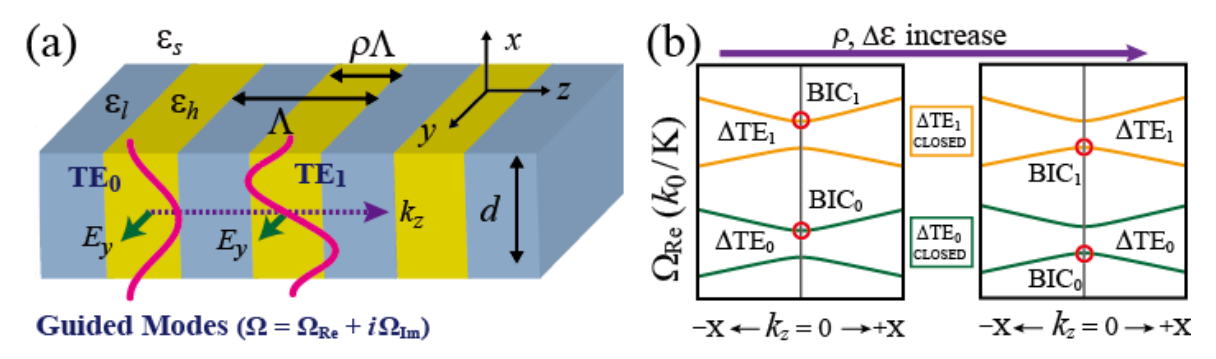


Figure 4. Definition of a simple lattice and a rendition of the band dynamics. (a) Schematic of a 1D leaky-mode photonic lattice for studying bound-state transitions. TE-polarized leaky guided modes are described by complex frequency $\Omega = \Omega_{Re} + i~\Omega_{Im}$. (b) Conceptual illustration of the bound-state transitions. Here, k_z is the wavevector along the z-direction and $X = \pi / \Lambda$. Before and after closing gaps ΔTE_0 and ΔTE_1 , symmetry-protected BIC₀ and BIC₁ in red circles appear at the upper and lower band edges, respectively. The BIC band edges are nonradiative and thus not leaky, whereas the opposite edges are leaky and represent the spectral placement of guided-mode resonance peaks. After ref. 45.

2.2 Band dynamics of resonant optical lattices

External waves incident on a periodic metamaterial lattice couple to it at frequencies corresponding to the leaky, or second, stop band. As shown above, the resulting resonance effects are useful in device design and spectral manipulation. Indeed, some of the most important properties of metamaterials are associated with the leaky stopband. The lattice band admits a leaky edge and a non-leaky edge for each supported resonant Bloch mode if the lattice is symmetric. The non-leaky edge

is associated with what is now called a bound state in the continuum (BIC), or embedded eigenvalue, currently of considerable scientific interest [39-43]. It is possible to control the width of the leaky band gap by lattice design. In particular, as a modal band closes, a quasi-degenerate state results—this state is remarkable as it is possible to transit to it by parametric and material choice. The transition to, and across, this point executes a band flip. We note that each lateral Bloch mode, in principle, possesses a band. The physical mechanisms inducing the band closure and the band flip are of fundamental interest [44, 45].

Figure 4 summarizes these ideas, applying a single 1D periodic membrane possessing thickness d with binary dielectric-constant modulation residing in a host medium with dielectric constant ε_s . The periodic layer acts as a waveguide as well as a phase-matching element because its average dielectric constant $\varepsilon_{avg} = \varepsilon_l + \rho(\varepsilon_h - \varepsilon_l)$ is larger than ε_s , where ε_h and ε_l represent the high and low dielectric constants, respectively, and ρ =F is the fill factor. The normally incident light is in the TE polarization state. The leaky bands of the fundamental TE₀ and first higher-order TE₁ modes are of interest here. As schematically shown in Fig. 1(b), the modal band gaps Δ TE₀ and Δ TE₁ belonging to TE₀ and TE₁ modes, respectively, are opened at $k_z = 0$ and symmetry-protected bound states BIC₀ and BIC₁ in red circles appear at the upper band edges of the bands when ρ and $\Delta\varepsilon$ are small. At particular values of ρ and $\Delta\varepsilon$, each band closes. The spectral locations of BIC₀ and BIC₁ transit from the upper to the lower band edges as the values of ρ and/or $\Delta\varepsilon$ increase [45].

It has been shown that the frequency location of the guided-mode resonance band edge, as well as the BIC edge, is determined by superposition of Bragg processes denoted by BR_{Q,n} where Q indicates the Bragg order and n denotes the Fourier harmonic of the dielectric constant modulation [44]. As a numerical illustration, we present an example of the attendant band dynamics and band flip in Fig. 5. The real part of frequency vs k defines the band structure. In general, band gaps corresponding to each guided mode appear as fill factor $0 < \rho < 1$ and modulation $\Delta \epsilon = \epsilon_h - \epsilon_l > 0$; here, we treat only the TE₀ band with a fixed fill factor F= ρ =0.48 as a function of modulation. It is shown in Fig. 5(a) that as $\Delta \epsilon$ grows, the band opens, closes, and reopens. The band closes when the two Bragg reflections BR_{2,1} and BR_{1,2} are balanced destructively [39]. Figure 5(b) shows corresponding plots of the imaginary part of the frequency versus real frequency. Before band flip, the upper edge has $\Omega_{lm} = 0$ which defines the BIC state as this condition denotes no leakage; i. e. this is the nonleaky band edge. In contrast, the finite value of Ω_{lm} at the lower edge implies leakage; this is the leaky band edge where the GMR peak arises with R₀=1 in principle. Beyond band closure, the BIC/GMR edges interchange, thus executing a band flip, as seen in Fig. 5(b) as well.

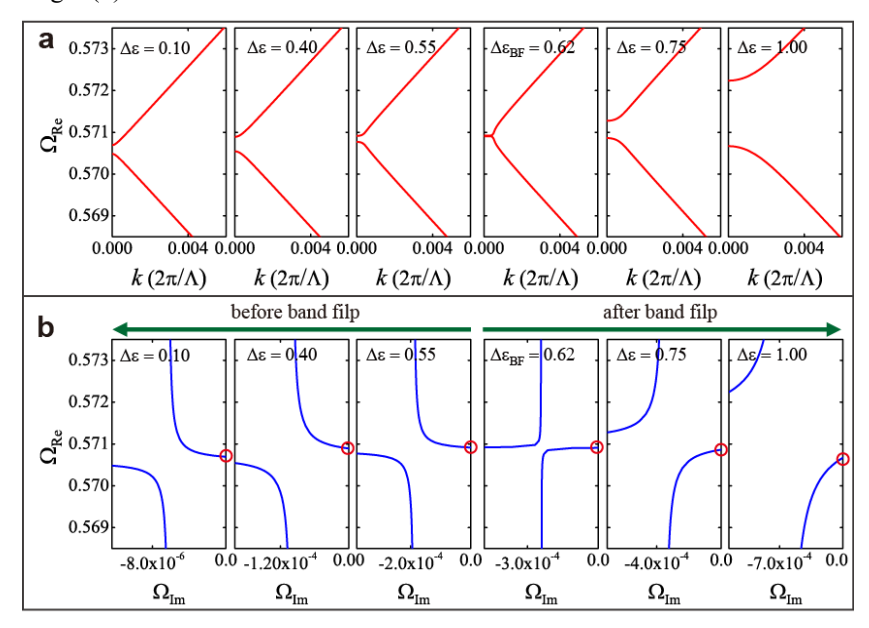


Figure 5. Illustration of the band dynamics associated with a lattice similar to that in Fig. 4 for the fundamental mode. The parameters are $\varepsilon_{avg} = 4$, $d = 0.50 \Lambda$, $\varepsilon_c = 1$; this lattice is on a substrate with $\varepsilon_s = 2.25$. (a) Band structure and band dynamics as a function of modulation strength $\Delta \varepsilon$. (b) Illustration of band-edge locations and band flips of the leaky GMR edge and the nonleaky BIC edge as correlated with the band dynamics in (a).

3. EXAMPLE APPLICATIONS

3.1 Wideband reflector at IR bands

Resonant reflectors can be designed to operate in arbitrary spectral regions. Operational principles and design methodology remain the same but actual fabrication methodology will vary widely with operational frequency and associated materials that must remain low-loss in the particular region of choice. Figure 6 shows an example device design operating as a wideband reflector in the 3-5 μm region. Reflectance is close to 100% across ~1.5 μm bandwidth.

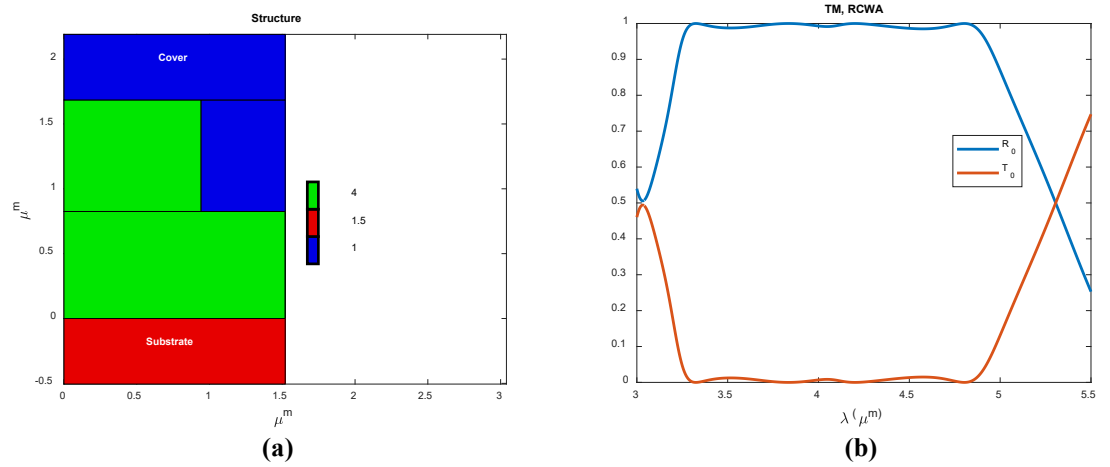


Figure 6. An example wideband reflector in the 3-5 μm region. (a) Schematic illustration of device structure denoting refractive indices used. Parameters set is { Λ =1.52 μm , F=0.62, d_g=860 nm, d_h=825 nm; TM polarization}. (b) Zero-order reflectance and transmittance spectra.

3.2 Wideband reflector with triangular profile

Photonic structures with nearly arbitrary periodic profiles can be used to induce the resonance effects under study herein [46]. To emphasize this point, shown in Fig. 7 are spectral maps for devices with triangular profiles as noted in the inset. The maps show zero-order reflectance as a function of homogeneous sublayer thickness d_h . Two distinct materials form the reflectors in Figs. 7(a) and 7(b). The widest available high-reflectance bands are marked by dotted lines in each case. Note that a resonant grating composed of isolated triangular particles at d_h =0 can provide substantial reflection bands; in Fig. 7(a) this bandwidth exceeds 100 nm, whereas in Fig. 7(b), it spans 400+ nm.

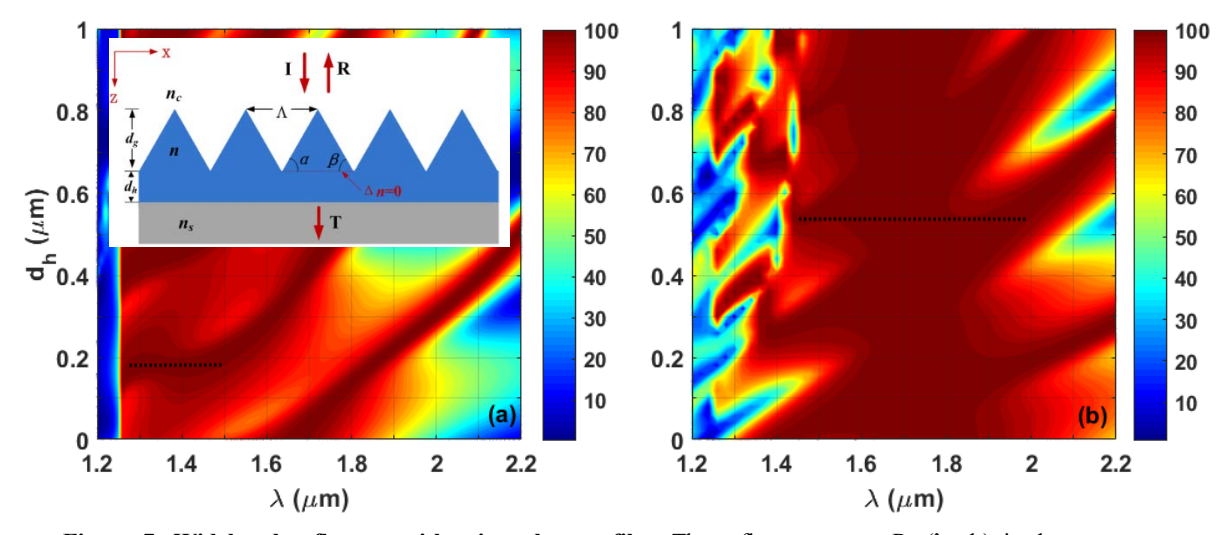


Figure 7. Wideband reflectors with triangular profiles. The reflectance map R_0 (λ , d_h) is drawn versus wavelength and thickness for period $\Lambda=850$ nm. (a) Base angles $\alpha=\beta=59^\circ$, $n_c=1$, n=3, and $n_s=1.48$; (b) Base angles $\alpha=\beta=58^\circ$, $n_c=1$, n=3.48, and $n_s=1.48$. Color scales denote levels of reflectance in percent. After ref. 46.

3.3 Silicon reflector in the visible region

Silicon has a complex refractive index close to n_c = n+ik=4+i0.04 in the visible spectral region near λ =550 nm. We design a resonant reflector to operate across a wide band centered at 550 nm. With reference to Fig. 1(a), the parameter set obtained is { Λ =315 nm, F=0.26, D_g =100 nm, D_h =16 nm; TE polarization}. Assuming first that k=0, a flat band results with zero-order reflectance R_0 =1, as seen in Fig. 8. Taking the native value for k=0.04, there is a significant drop in reflectance. It is well established that treatment with hydrogen (H_2) plasma can passivate deep level traps and defects in semiconductors [47]. Thus we proceed to hydrogenate films of silicon and reach a value of k=0.02, as measured in our labs with ellipsometry. This reduction in the k value improves the reflectance as modeled in Fig. 8. Further reduction of k would impact prospects for efficient silicon-based reflectors and other resonance devices in the visible region.

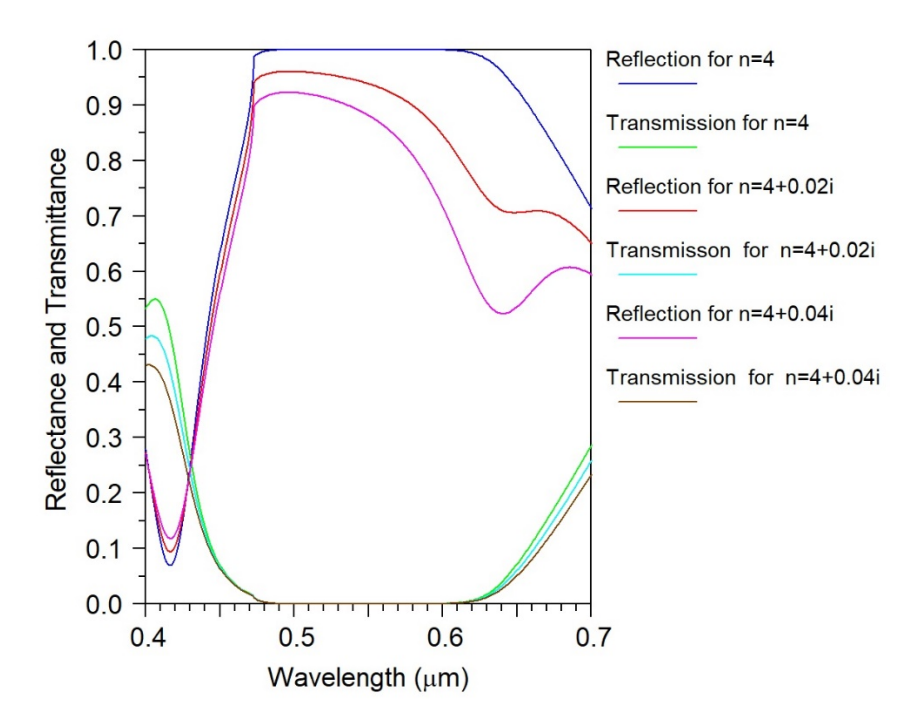


Figure 8. Spectral characteristics of a silicon reflector in the visible region. The value of reflectance relative to $Im(n_c)$ is quantified.

3.4 Polarizers with record performance

We have designed and fabricated compact low-loss, ultra-high extinction ratio polarizers based on multilayer resonant periodic metasurfaces [48]. The building block of the cascaded device is an individual metasurface polarizer containing subwavelength periodic patterns of crystalline silicon on top of a quartz substrate. These metasurfaces are fundamentally GMR grids. Cascading all-dielectric low-loss individual polarizers offers superior performance compared to the conventional bulky and lossy polarizers as we confirm by rigorous computations. The design possesses an appropriate angular tolerance of the transmission spectra for both TE and TM polarization states. Moreover, we experimentally verified the improved efficiency of our stacked multi-metasurface polarizer device. The thin air-gap thickness between the individual polarizers is controlled by the thickness of spin-coated photoresist which acts as a spacer. Our measured data shows an ultra-high extinction ratio of ~100,000 for a polarizer device containing two stacked double-grating modules which confirms the low-loss nature of our polarizer. As the patterned structures are enclosed by the quartz substrates and are therefore isolated from the surrounding environment, the risk of contamination or damage during handling is minimized. Figure 8 summarizes these points and main results.

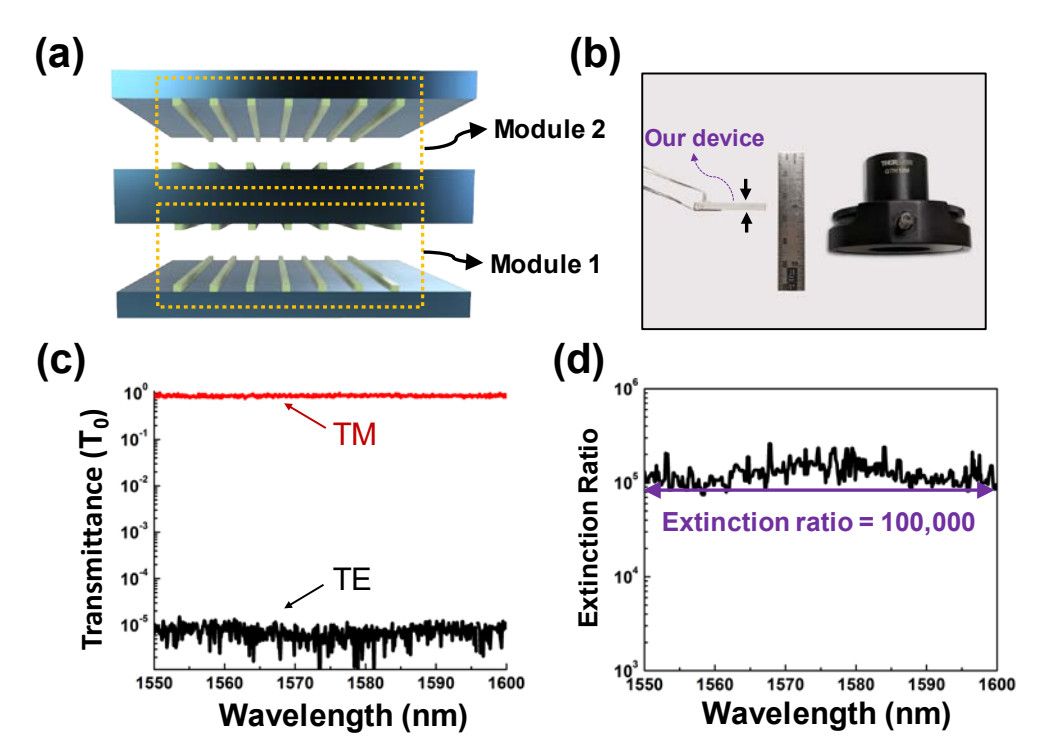


Figure 9. A fabricated stacked multi-metasurface polarizer. (a) Schematics of a device containing two dual-metasurface polarizer modules. (b) Photograph of our polarizer and Thorlab's Glan-Thompson polarizer. (c) Log-scale transmission spectra for TE and TM polarization states. (d) Extinction ratio of the fabricated polarizer. After ref. 48.

4. CONCLUSIONS

In conclusion, we present herein the principal aspects of leaky-mode photonic lattices that are the major building blocks of metamaterials, metasurfaces, and photonic crystal slabs. We explain key properties with strong reference to propagation of lateral Bloch modes. The lattices treated are periodic and possess waveguiding properties such that quasi-guided modes with finite lifetimes are sustained. It is widely acknowledged that the attendant spectral control enables numerous device applications with new attributes relative to prior technology including thin films, simple waveguides, and classic diffractive optics. We note that the one-dimensional grating-type canonical model is conceptually transparent, while encompassing all essential attributes applicable to two-dimensional metasurfaces and periodic photonic slabs. We emphasize the operative physical mechanisms grounded in lateral leaky Bloch mode resonance, accentuating the significant influence imparted by the periodicity and the waveguide characteristics of the lattice. The operative mechanisms and resulting properties are not explainable in terms of local Fabry-Perot or Mie resonances. In fact, with several definitive examples, we demonstrate that Mie scattering is not causative in resonant reflection. Applications presented include a wideband reflector at infrared bands as well as resonant reflectors with triangular profiles. We quantify improved efficiency of a silicon reflector operating in the visible region relative to loss reduction as realizable with hydrogenation. The spectral characteristics including extinction ratio of a resonant polarizer with record performance are presented.

ACKNOWLEDGEMENTS

This research was supported, in part, by the UT System Texas Nanoelectronics Research Superiority Award funded by the State of Texas Emerging Technology Fund as well as by the Texas Instruments Distinguished University Chair in Nanoelectronics endowment. Additional support was provided by the National Science Foundation (NSF) under Awards No. ECCS-1606898, ECCS-1809143, and IIP-1826966.

REFERENCES

- [1] P. Vincent and M. Neviere, "Corrugated dielectric waveguides: a numerical study of the second-order stop bands," Appl. Phys. 20, 345-351 (1979).
- [2] E. Popov, L. Mashev, and D. Maystre, "Theoretical study of the anomalies of coated dielectric gratings," Optica Acta 33, 607-619 (1986).
- [3] I. A. Avrutsky and V. A. Sychugov, "Reflection of a beam of finite size from a corrugated waveguide," J. Mod. Opt. 36, 1527-1539 (1989).
- [4] G. A. Golubenko, A. S. Svakhin, V. A. Sychugov, and A. V. Tishchenko, "Total reflection of light from a corrugated surface of a dielectric waveguide," Sov. J. Quantum Electron. 15, 886-887 (1985)
- [5] H. Kikuta, H. Toyota, and W. Yu, "Optical elements with subwavelength structured surfaces," Opt. Rev. 10, 63-73 (2003).
- [6] S. Wang and R. Magnusson, "Theory and applications of guided-mode resonance filters," Appl. Opt., 32, 2606-2613 (1993).
- [7] Y. Ding and R. Magnusson, "Resonant leaky-mode spectral-band engineering and device applications," Opt. Express 12, 5661-5674 (2004).
- [8] R. Magnusson and S. S. Wang, "New principle for optical filters," Appl. Phys. Lett. 61, 1022-1024 (1992).
- [9] W. Suh and S. Fan, "All-pass transmission or flattop reflection filters using a single photonic crystal slab," Appl. Phys. Lett. 84, 4905-4907 (2004).
- [10] R. F. Kazarinov and C. H. Henry, "Second-order distributed feedback lasers with mode selection provided by first-order radiation losses," IEEE J. Quantum Electron. QE-21, 144-150 (1985).
- [11] D. Rosenblatt, A. Sharon, and A. A. Friesem, "Resonant grating waveguide structures," IEEE J. Quantum Electron. 33, 2038-2059 (1997).
- [12] T. Tamir and S. Zhang, "Resonant scattering by multilayered dielectric gratings," J. Opt. Soc. Am. A 14, 1607-1616 (1997).
- [13] Y. Ding and R. Magnusson, "Band gaps and leaky-wave effects in resonant photonic-crystal waveguides," Opt. Express 15, 680-694 (2007).
- [14] D. Gerace and L. C. Andreani, "Gap maps and intrinsic diffraction losses in one-dimensional photonic crystal slabs," Phys. Rev. E 69, 056603 (2004).
- [15] Philippe Lalanne, Jean Paul Hugonin, and Pierre Chavel, "Optical properties of deep lamellar gratings: A coupled Bloch-mode insight," Journal of Lightwave Technology 24, 2442-2449 (2006).
- [16] K. J. Lee, R. L. Comb, B. Britton, M. Shokooh-Saremi, H. Silva, E. Donkor, Y. Ding, and R. Magnusson, "Siliconlayer guided-mode resonance polarizer with 40-nm bandwidth," IEEE Photonics Technol. Lett. 20, 1857-1859 (2008).
- [17] R. Magnusson, D. Wawro, S. Zimmerman and Y. Ding, "Resonant photonic biosensors with polarization-based multiparametric discrimination in each channel," Sensors 11, 1476-1488 (2011).
- [18] H. Wu, J. Hou, W. Mo, D. Gao, and Z. Zhou, "A broadband reflector using a multilayered grating structure with multi-subpart profile," Appl. Phys. B 99, 519–524 (2010).
- [19] S. Peng and G. M. Morris, "Resonant scattering from two-dimensional gratings," J. Opt. Soc. Am. A 13, 993-1005 (1996).
- [20] R. Magnusson, "Wideband reflectors with zero-contrast gratings," Opt. Lett. 39, 4337-4340 (2014).
- [21] C. F. R. Mateus, M. C. Y. Huang, Y. Deng, A. R. Neureuther, and C. J. Chang-Hasnain, "Ultrabroadband mirror using low-index cladded subwavelength grating," IEEE Photon. Technol. Lett. 16, 518–520 (2004).
- [22] Mohammad J. Uddin, Tanzina Khaleque, and Robert Magnusson, "Guided-mode resonant polarization-controlled tunable color filters," Optics Express 22, 12307–12315 (2014).
- [23] Kyu J. Lee, James Curzan, Mehrdad Shokooh-Saremi, and Robert Magnusson, "Resonant wideband polarizer with single silicon layer," Applied Physics Letters 98, 211112-1–211112-3 (2011).
- [24] Jae Woong Yoon, Kyu Jin Lee, and Robert Magnusson, "Ultra-sparse dielectric nanowire grids as wideband reflectors and polarizers," Optics Express 23, 28849-28856 (2015).
- [25] Yeong Hwan Ko, Kyu Jin Lee, and Robert Magnusson, "Experimental demonstration of wideband multimodule serial reflectors," Optics Express 25, 8680-8689 (2017).
- [26] Manoj Niraula, Jae Woong Yoon, and Robert Magnusson, "Concurrent spatial and spectral filtering by resonant nanogratings," Optics Express 23, 23428-23435 (2015).
- [27] Manoj Niraula, Jae Woong Yoon, and Robert Magnusson, "Single-layer optical bandpass filter technology," Optics Letters 40, 5062-5065 (2015).

- [28] Robert Magnusson, Debra Wawro, Shelby Zimmerman, and Yiwu Ding, "Resonant Photonic Biosensors with Polarization-based Multiparametric Discrimination in Each Channel," Sensors: Special Issue Optical Resonant Sensors 11, 1476–1488 (2011).
- [29] Yeong Hwan Ko and Robert Magnusson, "Wideband dielectric metamaterial reflectors: Mie scattering or leaky Bloch mode resonance?," Optica 5, 289-294 (2018).
- [30] S. S. Wang, R. Magnusson, J. S. Bagby, and M. G. Moharam, "Guided-mode resonances in planar dielectric layer diffraction gratings," J. Opt. Soc. Am. A 7, 1470-1474 (1990).
- [31] B. Slovick, Z. G. Yu, M. Berding, and S. Krishnamurthy, "Perfect dielectric-metamaterial reflector," Phys. Rev. B 88, 165116 (2013).
- [32] P. Moitra, B. A. Slovick, Z. G. Yu, S. Krishnamurthy, and J. Valentine, "Experimental demonstration of a broadband all-dielectric metamaterial perfect reflector,", Appl. Phys. Lett. 104, 171102 (2014).
- [33] Y. F. Yu, A. Y. Zhu, R. Paniagua-Domínguez, Y. H. Fu, B. Luk'Yanchuk, and A. I. Kuznetsov, "High transmission dielectric metasurface with 2π phase control at visible wavelengths," Laser Photon. Rev. 9, 412-418 (2015).
- [34] Pengfei Qiao, Weijian Yang, and Connie J. Chang-Hasnain, "Recent advances in high-contrast metastructures, metasurfaces, and photonic crystals," Adv. Opt. Photon. 10, 180-245 (2018).
- [35] A. Arbabi, E. Arbabi, Y. Horie, S. M. Kamali, and A. Faraon, "Planar metasurface retroreflector," Nat. Photonics 11, 415–420 (2017).
- [36] S. M. Kamali, E. Arbabi, A. Arbabi, Y. Horie, and A. Faraon, "Highly tunable elastic dielectric metasurface lenses," Laser Photon. Rev. 10, 1002–1008 (2016).
- [37] Wei Ting Chen, Alexander Y. Zhu, Vyshakh Sanjeev, Mohammadreza Khorasaninejad, Zhujun Shi, Eric Lee and Federico Capasso, "A broadband achromatic metalens for focusing and imaging in the visible," Nature Nanotechnology 13, 220 (2018).
- [38] Giorgio Quaranta, Guillaume Basset, Olivier J. F. Martin, Benjamin Gallinet, "Recent advances in resonant waveguide gratings," Laser & Photonics Reviews 12, 1800017 (2018).
- [39] A. Kodigala, T. Lepetit, Q. Gu, B. Bahari, Y. Fainman, and B. Kanté, "Lasing action from photonic bound states in continuum," Nature 541, 196–199 (2017).
- [40] J. Gomis-Bresco, D. Artigas and L. Torner, "Anisotropy-induced photonic bound states in the continuum," Nature Photonics 11, 232-236 (2017).
- [41] C. W. Hsu, B. Zhen, A. D. Stone, J. D. Joannopoulos, and M. Soljacic, "Bound states in the continuum", Nature Reviews Materials 1, 1–13 (2016).
- [42] D. C. Marinica, A. G. Borisov, and S. V. Shabanov, "Bound states in the continuum in photonics," Phys. Rev. Lett. 100, 183902 (2008).
- [43] Hafez Hemmati and Robert Magnusson, "Dual-grating metamaterials supporting spectrally narrow bound states in the continuum," Adv. Optical Mater. 7, 1900754 (2019).
- [44] Sun-Goo Lee and Robert Magnusson, "Band flips and bound-state transitions in leaky-mode photonic lattices," Phys. Rev. B 99, 045304 (2019).
- [45] Sun-Goo Lee and Robert Magnusson, "Band dynamics of leaky-mode photonic lattices," Optics Express 27, 18180-18189 (2019).
- [46] Shanwen Zhang, Yeong Hwan Ko, and Robert Magnusson, "Broadband guided-mode resonant reflectors with quasi-equilateral triangle grating profiles," Optics Express 25, 28451-28458 (2017).
- [47] M. T. Sultan, J. T. Gudmundsson, A. Manolescu, T. Stoica, M. L. Ciurea, and H. G. Svavarsson, "Enhanced photoconductivity of embedded SiGe nanoparticles by hydrogenation," Applied Surface Science 479, 403-409 (2019).
- [48] Hafez Hemmati, Pawarat Bootpakdeetam, and Robert Magnusson, "Metamaterial polarizer providing principally unlimited extinction," Opt. Lett. 44, 5630-5633 (2019).